


Available online at www.sciencedirect.com
ScienceDirect
Procedia IUTAM 14 (2015) 337 – 343
Procedia IUTAM
www.elsevier.com/locate/procedia

IUTAM_ABCM Symposium on Laminar Turbulent Transition

A dynamic observer to capture and control perturbation energy in noise amplifier flows

J. Guzmán Iñigo[a,*], D. Sipp[a], P. J. Schmid[b]

[a] *ONERA- The French Aerospace Lab, 8 rue des Vertugadins, 92190 Meudon, France*
[b] *Dept. of Mathematics, Imperial College London, London SW7 2AZ, United Kingdom*

Abstract

In this article, we present a technique to extract a reduced-order model of a transitional flat-plate boundary layer from simultaneous velocity snapshots and wall-shear stress measurements. The proposed approach combines a reduction of the degrees of freedom of the system by a projection of the velocity snapshots onto a POD basis together with a system-identification technique to obtain a state-space model of the flow. Such a model is then used in an optimal control framework to reduce the kinetic energy of the perturbation field and therefore delay transition.

Selection and peer-review under responsibility of ABCM (Brazilian Society of Mechanical Sciences and Engineering)
Keywords: Boundary layer control, Control theory, Drag reduction

1. Introduction

Closed-loop control, where actuation depends on sensor measurements, has the potential to become an effective method to delay laminar to turbulent transition in boundary layers[1,2]. Yet the implementation of such closed-loop control to realistic flows remains quite challenging. The main difficulty arises from the large number of degrees of freedom of fluid systems (often $O(10^6)$) which are far beyond the capabilities of current control devices. As a consequence, the full fluid system has to be properly reduced, before a controller can be designed for the reduced-order model. In[3] the model reduction is accomplished by a flow decomposition (e.g., POD or BPOD decomposition) followed by a Galerkin projection of the equations onto the reduced basis. This methodology has been demonstrated to yield successful control designs, see[1,4], among others.

In the case of boundary layers (and generally noise amplifier flows), external perturbations strongly influence the system dynamics. It is thus very important for the reduced-order model (ROM) to accurately capture the noise environment. ROMs obtained by means of Galerkin projections require detailed knowledge of the spatial distribution of the upstream noise sources. This requirement imposes great limitations, particularly in experimental situations where information about the noise environment is not directly and sufficiently available.

* Corresponding author.
E-mail address: juan.guzman_inigo@onera.fr

Selection and peer-review under responsibility of ABCM (Brazilian Society of Mechanical Sciences and Engineering)
doi:10.1016/j.piutam.2015.03.057

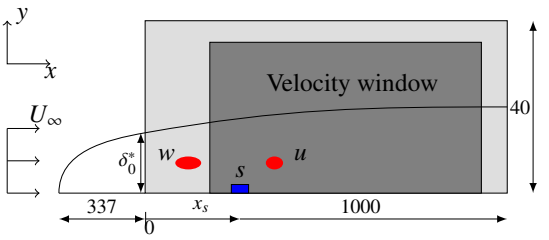

Fig. 1: Sketch of the flow configuration. The computational domain $\Omega = (0, 1000) \times (0, 40)$ is represented by the light gray box. The upstream receptivity of the boundary layer to external perturbations is modeled by the noise w which is placed at $(x_w, y_w) = (50, 0.95)$. A sensor located at $(x_s, y_s) = (200, 0)$ will identify incoming perturbations, while a velocity window (represented by the dark gray box) quantifies the effect of the forcing on the velocity field. A controller u is also introduced in the simulation at the position $(x_u, y_u) = (250, 1)$.

This paper intends to provide a methodology to obtain reduced-order estimators for noise amplifier flows without using Galerkin projections. The alternative approach is based on the extraction of the reduced-order model from measured data using an identification technique.

The proposed methodology constitutes a reduction of the degrees of freedom of the system by (i) a projection of the velocity fields onto a reduced basis combined with (ii) a system-identification algorithm to obtain the dynamic operators of a reduced-order system. In particular, a link between velocity fields (e.g., from TR-PIV data) and time-synchronous wall-shear stress measurements is established, and a dynamic observer is determined.

2. Configuration

We consider the dynamics of disturbances $\mathbf{u}$ around a base-flow $\mathbf{U}_0$, which we take as a Blasius boundary layer. The disturbances $\mathbf{u}$ are additionally driven by an external forcing term, $\mathbf{F}_w w(t)$, which acts as an upstream disturbance source of unknown origin. The spatio-temporal evolution of the perturbation flow-field $\mathbf{u}$ are governed by the following equations

$$\partial_t \mathbf{u} + \mathbf{U}_0 \cdot \nabla \mathbf{u} + \mathbf{u} \cdot \nabla \mathbf{U}_0 = -\nabla p + Re_{\delta_0^*}^{-1} \Delta \mathbf{u} + \mathbf{F}_w w(t), \qquad \nabla \cdot \mathbf{u} = 0, \tag{1}$$

where the nonlinear term $\mathbf{u} \cdot \nabla \mathbf{u}$ has been omitted since only low-amplitude noise $\sigma_w \ll 1$ will be considered. This assumption ensures a linear perturbation dynamics, as well as a linear response to the noise w. These equations (1) are solved in a computational domain Ω of size $(0, 1000) \times (0, 40)$, sketched in figure 1.

The variables are non-dimensionalized using the displacement thickness δ_0^* of the boundary-layer at the computational inlet ($x_0 = 0$) and the free-stream velocity U_∞. Consequently, the Reynolds number is defined as $Re_{\delta_0^*} = U_\infty \delta_0^* / \nu$. All simulations were performed at $Re_{\delta_0^*} = 1000$, which ensures the presence of strong Tollmien-Schlichting instabilities.

The approach proposed in this paper aims at being applicable in an experimental setting. For this reason, special care has been taken to only use data which is readily available in an experiment. We consider two elements to obtain information from the flow: a wall-friction sensor s and velocity snapshots $\mathbf{u}_{\text{snap}}$ in a given domain Ω_{snap}(see figure 1). In an experimental setup, the velocity snapshots could be obtained by a PIV technique.

3. A dynamic observer using system-identification techniques

A dynamic observer consists of a mathematical model of a fluid system which accurately predicts the dynamics of a flow from the measurement of a localized sensor. In this section we introduce a data-driven approach to obtain such a model, based on system identification techniques, that solely relies on observations of the system.

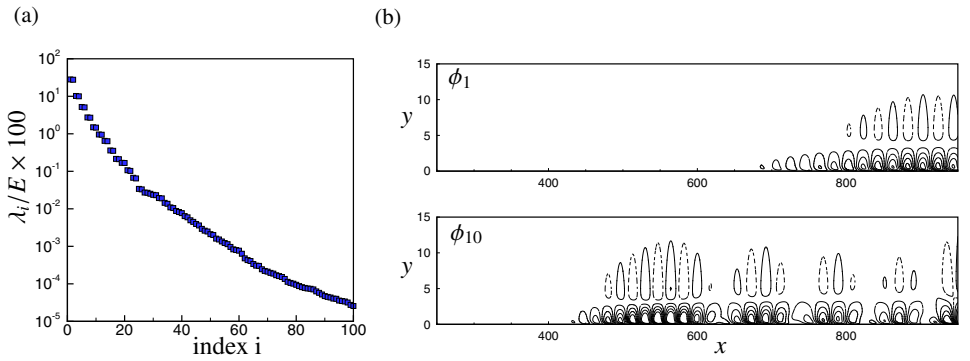

Fig. 2: (a) First 100 POD eigenvalues λ_i of the correlation matrix. (b) Contours of the streamwise velocity component of the first ($\mathbf{\Phi}_1$) and tenth ($\mathbf{\Phi}_{10}$) POD-mode.

3.1. Input and outputs of the system

System-identification techniques represent a family of algorithms which efficiently determine the coefficients of an underlying model directly from observed input-output data via a statistical learning process. In this case, the true input of the system is the driving term $w(t)$, while the true output is the velocity snapshot $\mathbf{u}_{\text{snap}}$ at each time instant. However, a direct identification of the system from them is not possible and different inputs and outputs must be considered.

The large number of degrees of freedom in the snapshots $\mathbf{u}_{\text{snap}}$ makes direct application of identification techniques excessively, or prohibitively, expensive. It is thus necessary to reduce the dimensionality of the measured data. In this article, we use the proper orthogonal decomposition (POD) modes [5,6] to form a reduced basis.

We consider a sequence of m velocity snapshots extracted from the Ω_{snap}-domain in the presence of the upstream noise w. The proper orthogonal decomposition then enables us to compute a ranked orthonormal basis $\{\mathbf{\Phi}_i\}_{i=1..m}$ of flow fields, satisfying $\left\langle \mathbf{\Phi}_i, \mathbf{\Phi}_j \right\rangle = \delta_{ij}, \quad i,j = 1,2,...,m$, which can be expressed most conveniently as a linear combination of these m snapshots. Here, the scalar-product $\langle\cdot\rangle$ is associated with the energy-based inner product: $\left\langle \mathbf{u}^1_{\text{snap}}, \mathbf{u}^2_{\text{snap}} \right\rangle = \int_{\Omega_{\text{snap}}} (u^1_{\text{snap}} u^2_{\text{snap}} + v^1_{\text{snap}} v^2_{\text{snap}})\, dx\, dy$. Any velocity field $\mathbf{V}$ in Ω_{snap} can then be projected onto the first k POD modes according to

$$y_i = \langle \mathbf{\Phi}_i, \mathbf{V} \rangle, \qquad i = 1,2,...,k, \tag{2a}$$

$$\mathbf{V}' = \sum_{i=1}^{k} \mathbf{\Phi}_i y_i, \tag{2b}$$

to produce the approximate flow field $\mathbf{V}'$. Properties of the POD guarantee that, for all k, the error $\|\mathbf{V} - \mathbf{V}'\|^2 = \langle \mathbf{V} - \mathbf{V}', \mathbf{V} - \mathbf{V}' \rangle$ is minimal for the set of m measured snapshots. For the subsequent derivations, we define the reduced state vector given by the k POD coefficients by $\mathbf{Y} = [y_1, y_2, ..., y_k]^T$ and denote the reduced POD basis by $\mathsf{U} = [\mathbf{\Phi}_1, \mathbf{\Phi}_2, ..., \mathbf{\Phi}_k]$.

Figure 2(a) shows the corresponding eigenvalues of the correlation matrix, confirming a steady decay over about three decades in the first thirty modes (95 % of the energy is contained in the first ten modes). Two selected POD modes, $\mathbf{\Phi}_1$ and $\mathbf{\Phi}_{10}$, are displayed in figure 2(b). The velocity snapshots $\mathbf{u}_{\text{snap}}$ are then projected onto these modes to obtain the time-evolving POD coefficients $\mathbf{Y}(n)$ which constitute the new output of the system.

On the other hand, it is critical to accurately account for the disturbance environment $w(t)$, as it both triggers and sustains the dynamics of the system. Despite this requirement, in an experimental setup, access to accurate information about the noise environment is, at best, very difficult or, in most cases, impossible. We thus have to introduce an observer where the noise source-term $w(t)$ is replaced by a measurement term $s(t)$ which drives, as best as possible, the estimated state of the system.

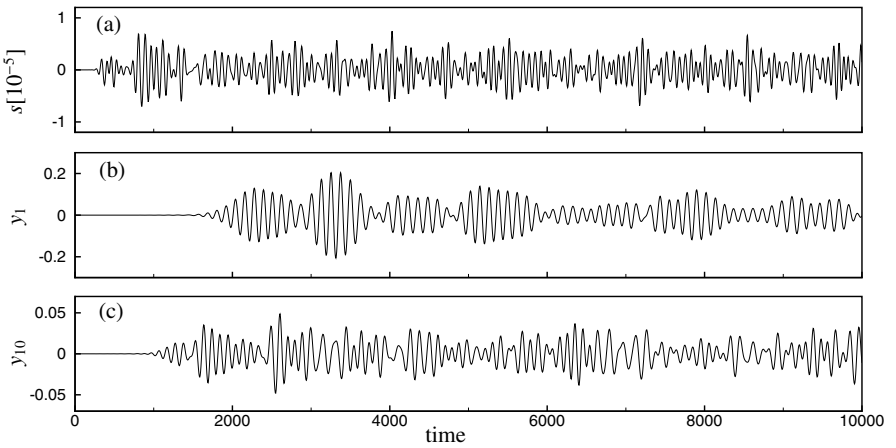

Fig. 3: Learning dataset: (a) the measurement s capturing the influence of external noise and (b) and (c) the POD coefficients y_i obtained by projecting the flow field onto the POD modes $\mathbf{\Phi_1}$ and $\mathbf{\Phi}_{10}$, respectively.

An approximation $\mathbf{Y}_e$ of the temporal evolution of the reduced state vector $\mathbf{Y}$ can be obtained by time marching a dynamic observer equation of the form

$$\mathbf{Y}_e(n+1) = \mathsf{A}_s \mathbf{Y}_e(n) + \mathbf{L}s(n). \tag{3}$$

The quantities A_s, $\mathbf{L}$ and $\mathbf{C}$ will be obtained with system identification techniques that solely rely on knowledge of input-output datasets $\{s(n), \mathbf{Y}(n)\}_{n=1..m}$.

3.2. System identification based on subspace techniques

Subspace identification algorithms are a very convenient choice when dealing with multiple-input-multiple-output (MIMO) systems, such as the one given in Eq. (3). In general, we have $u(n)$ as known inputs, $w(n)$ as unknown white plant noise and $y(n)$ as known outputs corrupted by unknown white noise $v(n)$. We aim at determining the system matrices ($\mathcal{A}, \mathcal{B}, C$ and $\mathcal{D}$), which govern a state $x(n)$ such that

$$x(n+1) = \mathcal{A}x(n) + \mathcal{B}u(n) + w(n), \tag{4a}$$

$$y(n) = Cx(n) + \mathcal{D}u(n) + v(n). \tag{4b}$$

The coefficients of the system matrices are chosen such that the estimated output $y_e(n)$, obtained by time-marching (4) with $w(n) = v(n) = 0$, is as close as possible to the measured output $y(n)$ (subject to the white-noise sources $w(n)$ and $v(n)$), knowing the inputs $u(n)$. A comprehensive description of these techniques is given in [7,8]. In this study, the `N4SID` algorithm [9] has been used to obtain all the models.

A relation between the elements of the dynamic observer (3) and the general formulation of subspace algorithms (4) can straightforwardly be defined as $\mathsf{A}_s = C\mathcal{A}C^{-1}$ and $\mathbf{L} = C\mathcal{B}$, assuming that $\mathcal{D} = 0$.

3.3. DNS-dataset for learning and testing

We obtain data by performing a linearized direct numerical simulation of the boundary layer in the presence of unknown noise. We use a sampling interval $\Delta t = 5$ for the velocity snapshots and the shear-stress measurements s. The datasets to be processed are composed of the input signal from the sensor s and several outputs y_i corresponding to the projection of the snapshots onto the set of POD modes $\{\mathbf{\Phi}_i\}$ (figure 3). Using the `N4SID` algorithm [9], the model parameters A_s and $\mathbf{L}$ are then determined by fitting the model output to the true, measured output, as the model is forced by the recorded input. A reduced-order model has been determined with $k = 90$ POD modes and a learning data set of length $N_{\text{snap}} = 2000$.

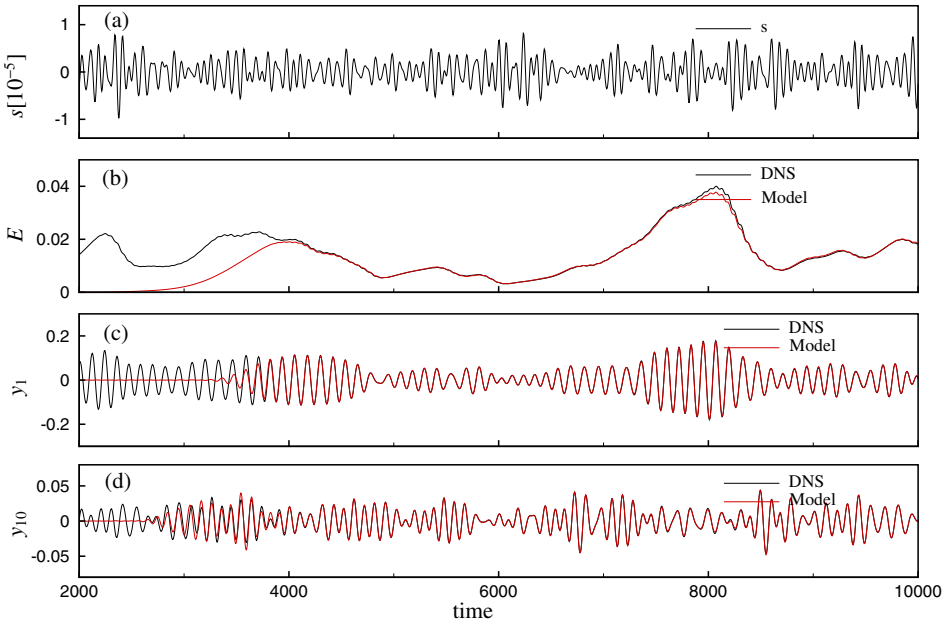

Fig. 4: Validation dataset: performance of the system-identified model, initialized by $\mathbf{Y} = 0$ at $t = 2000$. The input data from the wall shear-stress sensor s is shown in (a); the remaining flow variables are recovered solely from this measurement signal using the identified model. (b-d) Comparison between the DNS (black) and the model prediction (red) for four variables from the testing dataset: (b) the energy of the system, (c) and (d) the POD coefficients y_i for the first and tenth modes, respectively.

The validity of the identified parameters is subsequently confirmed by using a *different* data set (referred to as the testing data set) and by comparing the model output to the true output. As this testing data set has not been used in the identification of the model, we can assess the predictive capability of the identified model in this manner. The kinetic energy defined as $E(t) = \left\langle \mathbf{u}_{\text{snap}}, \mathbf{u}_{\text{snap}} \right\rangle \approx \mathbf{Y}^*\mathbf{Y}$ is an important variable of the system since it represents the global dynamics of the flow. The quality of fit between the energy of the DNS, denoted by $E(t)$, and the value predicted by the model, denoted by $\widetilde{E}(t)$, can be stated as

$$\mathsf{FIT}[\%] = 100\left(1 - \frac{\left\|E(t) - \widetilde{E}(t)\right\|}{\|E(t) - \text{mean}(E(t))\|}\right) \tag{5}$$

and can be used to quantify the performance of the estimator. Figure 4(a) displays the measured input signal s from the wall shear-stress sensor, from which all subsequent flow variables (figure 4(b-d)) can be derived using the identified model. In our case, we show the evolution of energy (b) and the first and tenth POD coefficient. After a short transient period, the predicted flow variables closely track their true DNS-equivalents, which yields a relative match of $\mathsf{FIT}_{\text{ener}} = 93.72\%$ when evaluated over the time interval $t \in [4000, 10000]$. From the POD coefficients in $\mathbf{Y}_e$ the full flow field can be reconstructed from the basis U. Two examples of this reconstruction, visualized by the streamwise velocity component, are shown in figure 5 and compared to the equivalent full DNS simulation. The first instant at $t = 3000$ has been taken during the transient phase and shows a promising but incomplete match over the entire flow domain; a second instant at $t = 4000$ displays an excellent agreement between the flow structure recovered from $s(t)$ via the identified model and the full DNS solution.

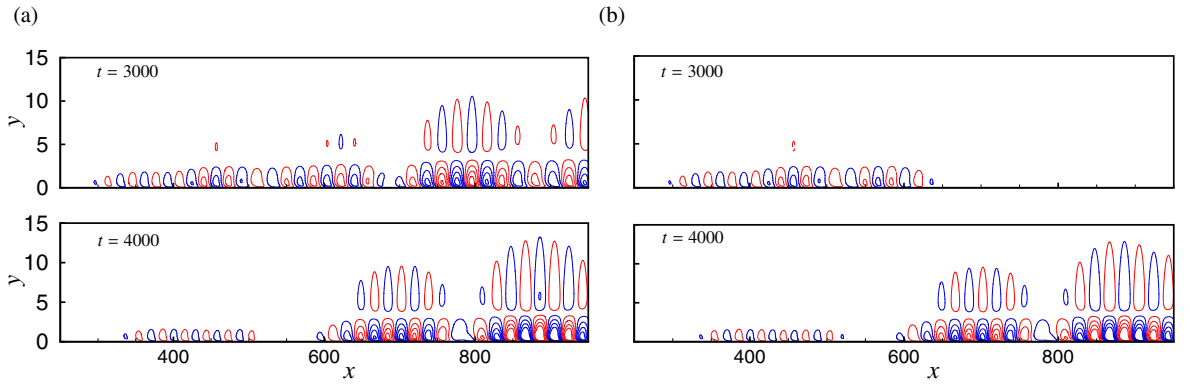

Fig. 5: Snapshots of the streamwise disturbance velocity component obtained (a) from the DNS and (b) recovered from $s(n)$ via the model for $t = 3000$ and $t = 4000$.

4. Optimal control

The successful recovery of full-state information from single wall shear-stress measurements by a dynamic observer enables the design of a variety of effective control schemes, which we demonstrate next. For this purpose, a control signal u is placed at $(x_u, y_u) = (250, 1)$ (downstream of the sensor s), which constitutes a feedforward control configuration. The governing equations (3) of the dynamic observer are modified to reflect this addition. We have

$$\mathbf{Y}_e(n+1) = \mathsf{A}_s\mathbf{Y}_e(n) + \mathbf{L}s(n) + \mathbf{B}_u u(n). \tag{6}$$

Following [10], the system is excited with a frequency-rich signal u in order to identify the new term $\mathbf{B}_u$. The unknown system matrices A_s, $\mathbf{L}$ and $\mathbf{B}_u$ may then be determined in a similar way as described in Sec. 3. These matrices are then used for the design of an LQR-optimal controller $u(n) = \mathbf{K}\mathbf{Y}(n)$, which minimizes the cost functional $\sum_{n=0}^{\infty} \mathbf{Y}(n)^*\mathsf{Q}\mathbf{Y}(n) + \ell^2|u(n)|^2$, where Q is a positive definite weight matrix and ℓ is a user-specified parameter to balance disturbance energy and exerted control energy. Following standard procedure (see [11]), the control gain $\mathbf{K}$ can be obtained by solving a Riccati equation involving A_s, $\mathbf{B}_u$, Q and ℓ.

The suppression of the perturbation energy $E(t)$ inside the velocity window ($\mathsf{Q} = \mathsf{I}$) has been considered as the control objective. We use a model that comprises 50 modes computed on a shorter domain ($\Omega_{\text{snap}} = (200, 700) \times (0, 40)$). In the controlled simulation, the measurement s is used to reconstruct the full perturbation field $\mathbf{Y}_e$ based on the identified model, and the control law is obtained by applying the control gain $\mathbf{K}$ to this state. Results are shown in figure 6 together with the control signal $u(t)$ and the friction-sensor signal s. The energy $E(t)$ has been reduced by nearly two orders of magnitude (a reduction of 96.81% in the mean perturbation energy).

5. Conclusion

A dynamic observer recovering full state information from single wall shear-stress measurements has been designed that relies on a POD basis (from measured snapshots) and system identification techniques. For noise-amplifier flows, it successfully reproduces the perturbation dynamics (velocity fields) throughout the full sampling domain and furnishes information about the flow that can subsequently be used, by itself, for flow diagnostics or, in a second step, for LQR-control design.

Within the limits of linear perturbation dynamics, the design process for the dynamic observer extracts the system matrix from a sequence of snapshots; this system matrix describes a globally stable flow configuration that is sustained by selectively amplified random perturbations from the noise environment. The proposed method thus successfully separates the intrinsic, stable perturbation dynamics from the external noise excitation, which previously could only be quantified in its entirety.

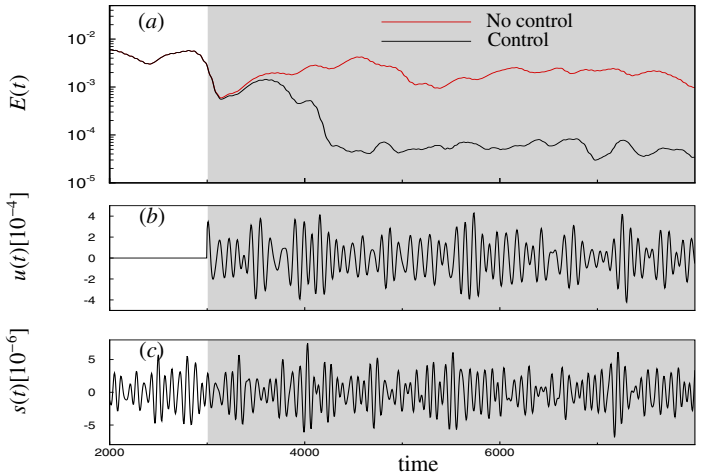

Fig. 6: Results of the LQR-control design based on the dynamic observer. (a) Temporal evolution of the perturbation energy $E(t)$ for the uncontrolled simulation (red) and the controlled simulation targeting the energy (black), (b) the control signal $u(t)$ and (c) the time signal of the friction sensor $s(t)$ used to estimate the state.

A wide variety of flow analyses is possible once the system matrix has been extracted. In the present case, we chose to design a closed-loop control scheme which, owing to the known system matrix, could now be accomplished using full information control (LQR) algorithms. As a consequence, a significant reduction of the perturbation energy could be achieved.

References

1. Bagheri, S., Brandt, L., Henningson, D.. Input–output analysis, model reduction and control of the flat-plate boundary layer. *J Fluid Mech* 2009;**620**(1):263–298.
2. Semeraro, O., Bagheri, S., Brandt, L., Henningson, D.S.. Feedback control of three-dimensional optimal disturbances using reduced-order models. *Journal of Fluid Mechanics* 2011;**677**:63–102.
3. Rowley, C.W.. Model reduction for fluids, using balanced proper orthogonal decomposition. *International Journal of Bifurcation and Chaos* 2005;**15**(03):997–1013.
4. Barbagallo, A., Sipp, D., Schmid, P.. Closed-loop control of an open cavity flow using reduced-order models. *J Fluid Mech* 2009; **641**(1):1–50.
5. Lumley, J.L.. The structure of inhomogeneous turbulent flows. *Atmospheric turbulence and radio wave propagation* 1967;:166–178.
6. Sirovich, L.. Turbulence and the dynamics of coherent structures. *Q Appl Math* 1987;**45**:561–571.
7. Qin, S.. An overview of subspace identification. *Comp & Chem Eng* 2006;**30**(10):1502–1513.
8. Van Overschee, P., De Moor, B.. *Subspace identification for linear systems*. Kluwer; 1996.
9. Van Overschee, P., De Moor, B.. N4SID: Subspace algorithms for the identification of combined deterministic-stochastic systems. *Automatica* 1994;**30**(1):75–93.
10. Hervé, A., Sipp, D., Schmid, P., Samuelides, M.. A physics-based approach to flow control using system identification. *J Fluid Mech* 2012;**702**:26–58.
11. Burl, J.B.. *Linear Optimal Control*. Addison-Wesley Longman Publishing Co., Inc.; 1999.